Light: Science & Applications (2017) 6, e16199; doi:10.1038/lsa.2016.199
Official journal of the CIOMP 2047-7538/17
www.nature.com/lsa

ORIGINAL ARTICLE

Quantum dot vertical-cavity surface-emitting lasers covering the 'green gap'

Yang Mei[1,*], Guo-En Weng[1,2,*], Bao-Ping Zhang[1], Jian-Ping Liu[3], Werner Hofmann[1,4], Lei-Ying Ying[1], Jiang-Yong Zhang[1], Zeng-Cheng Li[3], Hui Yang[3] and Hao-Chung Kuo[1,5]

Semiconductor vertical-cavity surface-emitting lasers (VCSELs) with wavelengths from 491.8 to 565.7 nm, covering most of the 'green gap', are demonstrated. For these lasers, the same quantum dot (QD) active region was used, whereas the wavelength was controlled by adjusting the cavity length, which is difficult for edge-emitting lasers. Compared with reports in the literature for green VCSELs, our lasers have set a few world records for the lowest threshold, longest wavelength and continuous-wave (CW) lasing at room temperature. The nanoscale QDs contribute dominantly to the low threshold. The emitting wavelength depends on the electron–photon interaction or the coupling between the active layer and the optical field, which is modulated by the cavity length. The green VCSELs exhibit a low-thermal resistance of 915 kW^{-1}, which benefits the CW lasing. Such VCSELs are important for small-size, low power consumption full-color displays and projectors.
Light: Science & Applications (2017) **6,** e16199; doi:10.1038/lsa.2016.199; published online 27 January 2017

Keywords: GaN; InGaN; quantum dot; vertical-cavity surface-emitting laser; wide-gap semiconductor

INTRODUCTION

Semiconductor lasers have attracted much attention since their invention in 1962[1,2]. Compared with solid state and gas lasers, semiconductor lasers have a small volume, low-operation current and voltage, and low cost. As determined by the band gaps of the variety of semiconductor materials, the wavelengths of semiconductor lasers can cover a wide spectral range, from violet to infrared[3]. Thus far, some of them have been well-studied and/or successfully commercialized, for example, ~2–5 μm lasers for biomedical and environmental applications[4], 1.3–1.55 μm lasers for optical fiber communications[5], 850–1000 nm lasers for optical interconnection and pumping sources[6–8], and 405–450 nm lasers for information recording, lithography, lighting, displays and projectors[9–12]. However, semiconductor lasers with wavelengths in the green region, typically 500–600 nm, are still undeveloped, which is called the 'green gap'[13]. The green light in this range is very important for a wide-gamut of applications. Presently, green lasers based on optical pumping or double-frequency technologies are usually adopted, but they are expensive and large.

A green semiconductor laser was first demonstrated by employing ZnSe-based semiconductors in the 1990s[14]. However, the lifetime of such devices was not sufficient for practical applications, and research on ZnSe is still ongoing[15]. In the last decades, much effort has been expended on GaN-based semiconductors. On the basis of these materials, a few types of optoelectronic devices such as light-emitting diodes and violet and blue lasers have been successfully demonstrated and commercialized[10,12,16,17]. Therefore, GaN-based semiconductors, including those of GaN, AlN, InN and their mixed alloys, are believed to be good candidates for green lasers. In 2009, Nichia[18] first broke the '500-nm limit' of green laser diodes, and then in the following 2 years, Osram[19], Sumitomo[20], Corning[21] and UCSB[22] pushed the wavelength up to 532 nm by using a c-plane and semipolar substrate. However, the expansion of the lasing wavelength is generally accompanied by an increase in the threshold current density, so the optimal filling of the 'green gap' has not been realized yet.

Two-dimensional InGaN quantum wells (QWs) are commonly used as the active region of violet, blue and green semiconductor lasers. The InGaN QW layer is sandwiched between GaN barriers. To obtain green emission lasers, a higher In content in the InGaN QW layer is necessary compared with that in the violet and blue lasers[3,13]. The existence of the 'green gap' is due mainly to the low-emission efficiency of the green InGaN QW layer. Defects and built-in electric fields in the QW are the dominant reasons accounting for the low-emission efficiency. Defects come from the lattice mismatch (or strain) between InGaN and GaN as well as between the epilayer and the substrate[23]. The built-in electric field originates from spontaneous polarization, which occurs when the QW is epitaxially grown on

[1]Department of Electronic Engineering, Optoelectronics Engineering Research Center, Xiamen University, Xiamen, Fujian 361005, China; [2]Department of Electronic Engineering, East China Normal University, Shanghai 200241, China; [3]Suzhou Institute of Nano-tech and Nano-bionics, Chinese Academy of Sciences, Suzhou, Jiangsu 215123, China; [4]School of Solid State Physics, Technical University of Berlin, Berlin 10623, Germany and [5]Department of Photonics and Institute of Electro-optical Engineering, Taiwan Chiao Tung University
*These authors contributed equally to this work.
Correspondence: BP Zhang, Email: bzhang@xmu.edu.cn; JP Liu, Email: jpliu2010@sinano.ac.cn
Received 22 April 2016; revised 11 August 2016; accepted 11 August 2016; accepted article preview online 19 August 2016

(0001) polar surfaces, and strain-induced piezopolarization[24]. To overcome these problems, epitaxial growth on homogeneous polar[25], semipolar[26] and nonpolar GaN substrates has been carried out[27]. However, these approaches cannot eliminate the strain between InGaN and GaN, and thereby the strain-induced defects and piezoelectric field in the InGaN QWs cannot be eliminated. This strain becomes pronounced when the In content is higher. In other words, InGaN QWs emitting in the green region have a lower emission efficiency than those emitting in the violet and blue regions.

To release the strain, the adoption of nanoscale quantum dots (QDs) is an effective approach. Semiconductor QDs can be formed during the epitaxial growth of a highly strained layer. The formation of QDs is driven by the strain itself, and the strain remaining in the QD can be significantly reduced compared with the case of a two-dimensional QW epitaxial layer[28]. QDs are zero-dimensional structures in which electrons and holes are strictly confined in a small volume, which is particularly important to obtaining a high-emission efficiency and low-threshold current, as reported in a few review papers[29–31]. Using InGaN QDs as the active region, green edge-emitting semiconductor lasers have been demonstrated by a research group at the University of Michigan[32]. Lasing actions were obtained even on lattice-mismatched substrates and polar surfaces. These results indicate the potential to fabricate lasers emitting in the 'green gap' by employing InGaN QDs.

The lasers mentioned above are edge-emitting lasers (EELs), in which the laser beam propagates parallel to the layer surface/interface. The cavity length is long, commonly a few hundred micrometers[33]. In this case, the separation of longitudinal modes, inversely proportional to the cavity length, is tiny, and the lasing wavelength is determined by the emission of the active region. Therefore, to shift the lasing wavelength, one has to prepare different structures for the active regions, for example, InGaN QDs with various In contents (0.18, 0.32 and 0.4 for blue, green and red, respectively)[34]. This not only complicates the fabrication process, especially the material growth, but also makes the laser expensive. On the other hand, vertical-cavity surface-emitting lasers (VCSELs), another type of semiconductor laser, can easily control the lasing wavelength by adjusting the cavity length. The cavity length of a VCSEL is much shorter, usually ~ 1 μm, and the mode separation is large and can be easily shifted by adjusting the cavity length. If the spontaneous emission band of the active layer is broad enough, one can obtain various lasing wavelengths by the proper design of the cavity. The laser beam of a VCSEL propagates vertical to the layer surface/interface.

There have been a few reports on GaN-based VCSELs using InGaN QW active regions[35–40]. Room temperature continuous-wave (CW) lasing has been demonstrated in the violet and blue region. However, in the green region, only pulsed lasing has been obtained, with wavelengths up to 503 nm[36]. In this paper, we report the first InGaN QD-based VCSELs. By a combination of InGaN QDs and vertical-cavity structures, we demonstrate VCSELs with different lasing wavelengths covering most of the 'green gap'. Different from InGaN QD EELs where different active structures are needed, we use the same epitaxial wafer grown on a (0001) polar surface by using a sapphire substrate. By controlling the cavity length, the lasing wavelength is shifted from 491.8 to 565.7 nm, with threshold currents of sub-mA. Moreover, room temperature CW lasing is obtained. The emission wavelength, threshold current and CW lasing are the record results for GaN-based VCSELs. The controllability of the emission wavelength is believed to be useful in full-color small-size laser displays and projectors.

MATERIALS AND METHODS

The epitaxial wafer was grown on a (0001) c-plane sapphire substrate using metal-organic chemical vapor deposition[41]. The epilayers include, in order, undoped GaN, n-type GaN, two layers of InGaN QDs and p-type GaN. The QDs with ~ 27% indium content have diameters ranging from 20 to 60 nm, and the average height is ~ 2.5 nm. The QD density is ~ 1.5E10 cm^{-2}. Figure 1a shows a $5 \times 5\ \mu m^2$ Atomic Force Microscope (AFM) image of the uncapped QDs. The device fabrication procedure is similar to that described in our previous work[37]. We first deposited a 100-nm-thick SiO_2 current insulation layer on the surface of the epitaxial wafer, and a 10-μm-diameter current-injection aperture was opened. Then, a 30-nm-thick indium tin oxide (ITO) ohmic contact and current spreading layer was deposited, followed by the formation of a Cr/Au p-electrode and a 12.5-pair TiO_2/SiO_2 bottom dielectric distributed Bragg reflector (DBR). The DBR was selectively deposited on the current-confinement aperture. After that, the sample was turned upside down and bonded onto a copper plate through a metal bonding technique, and then the sapphire substrate was detached by a laser lift-off process. An inductively coupled plasma etching technique was adopted to remove the undoped GaN layer. The n-GaN layer was thinned to a desired thickness, followed by chemical mechanical polishing to make the surface flat. Then, an n-contact metal and an 11.5-pair TiO_2/SiO_2 top dielectric DBR were deposited. A schematic structure of the green InGaN QD VCSEL is shown in Figure 1b, and a photo of the fabricated VCSEL array is given in Figure 1c. By controlling the thickness of the n-GaN layer, four samples were fabricated with different cavity lengths. Measurements of the lasing properties were performed at room temperature.

RESULTS AND DISCUSSION

We first calculated the cavity modes of the VCSEL using the matrix optics method. Figure 2a shows the calculated reflection spectrum of the GaN-based VCSEL and the measured photoluminescence (PL) spectrum of the QD wafer. The stopband of the DBR is ~ 150 nm, and it has seven cavity modes. The spontaneous emission of the QDs starts from 450 nm and ends at 600 nm. The broad spectrum is attributed to the inhomogeneity in the QD size and the fluctuation of the In content. The wide PL spectrum of the QDs is expected to allow VCSEL lasing at different wavelengths. The light-emission properties of the QD wafer were also studied using spatially resolved spot-focus cathodoluminescence (CL) at low temperature (4 K). CL spectra were measured through the 5-μm diameter apertures of a metal mask. We can clearly see some bright spots in the aperture. Figure 2b shows the CL image and the spectra recorded at bright spot A and other regions. A narrow emission peak is observed at position A, with a linewidth of 4 meV, much narrower than the PL given in Figure 2a. Due to the resolution limitation, the CL emission linewidth is not as small as the 107 μeV that was observed by others from a single InGaN QD[42]. Nevertheless, the emission property indeed proves the QD-like structure.

Figure 3a–3c shows the lasing spectra of three samples under different current levels, together with the corresponding light output–current (I–L) and current–voltage (I–V) characteristics. Figure 3d shows the polarized spectra of the fourth sample under 1 mA with different polarization angles. The polarization ratio turned out to be 91%, given by $(L_{max} - L_{min})/(L_{max} + L_{min})$, where L_{max} and L_{min} are the maximum and minimum relative light intensities, respectively. The lasing action under CW operation at room temperature was obtained for all the samples. This is the first report of the CW lasing of GaN-based green VCSELs at room temperature. Either double-longitudinal mode lasing (a, b, d)

doi:10.1038/lsa.2016.199

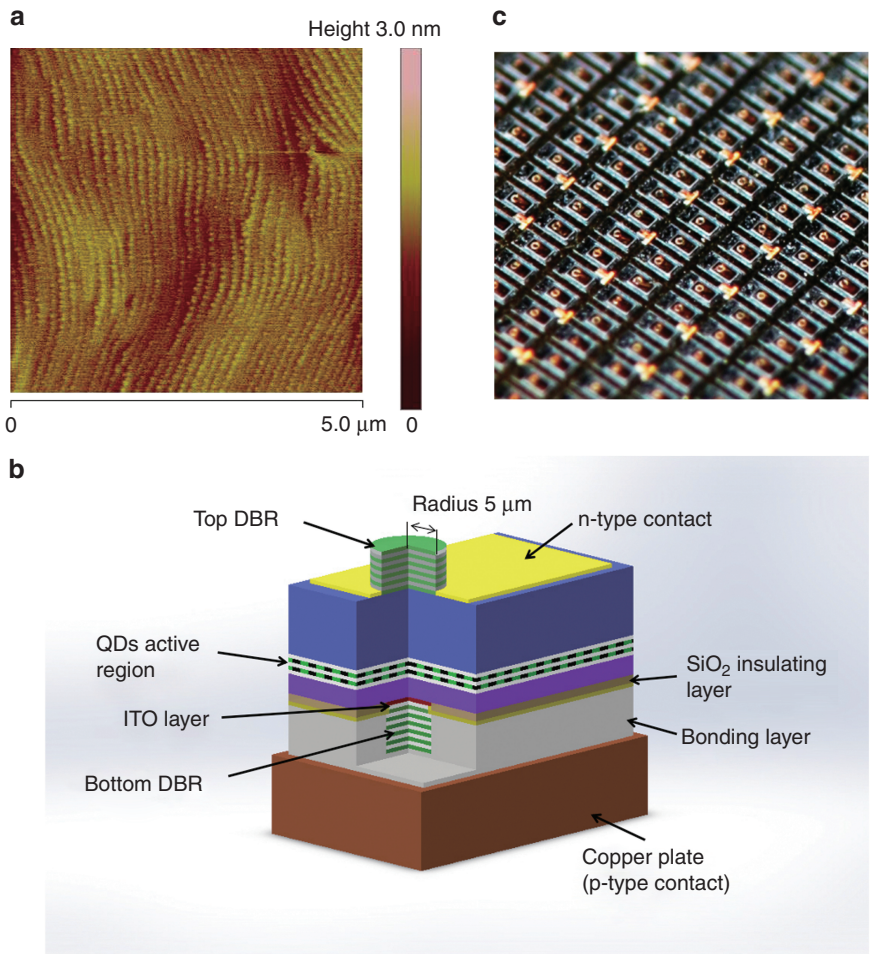

Figure 1 (**a**) A $5 \times 5\ \mu m^2$ AFM image of uncapped InGaN QD layer. (**b**) Schematic structure of the GaN-based VCSEL with a vertical current-injection configuration and QD active region. (**c**) Photo of the VCSEL array.

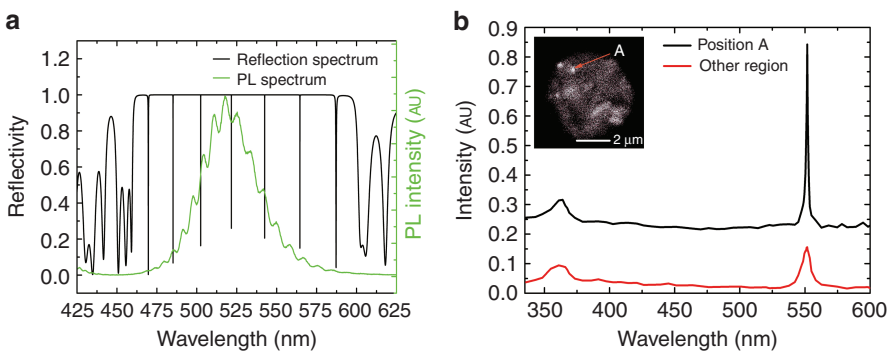

Figure 2 (**a**) Calculated reflection spectrum of the micro cavity and measured PL spectrum of the QD epitaxial wafer. (**b**) CL spectra from light spot A and other regions of the sample. Inset shows the CL image at 4 K.

or single-longitudinal mode lasing (c) was observed. Apart from the lasing peaks, other small peaks related to the cavity modes were also observed. It is clearly revealed from the lasing spectra that the intensities of the lasing peaks increased dramatically above the threshold current, and no mode hopping occurred, in spite of the existence of several additional longitudinal modes. The VCSELs have threshold currents of 0.52, 0.65 and 0.61 mA for (a), (b) and (c), respectively, corresponding to current densities of 0.66, 0.83 and 0.78 kA cm^{-2}. The slope efficiencies are 6.62, 7.64 and 11.82 mW A^{-1}, respectively. The lasing threshold currents and wavelengths are summarized in Figure 3e, along with the results reported in the literature on the QW active regions. The threshold current of our QD VCSELs is lower than that of any InGaN QW VCSEL ever reported, whether violet, blue or green. The lasing wavelengths of our QD VCSELs were 491.8–565.7 nm, covering most of the 'green gap'.

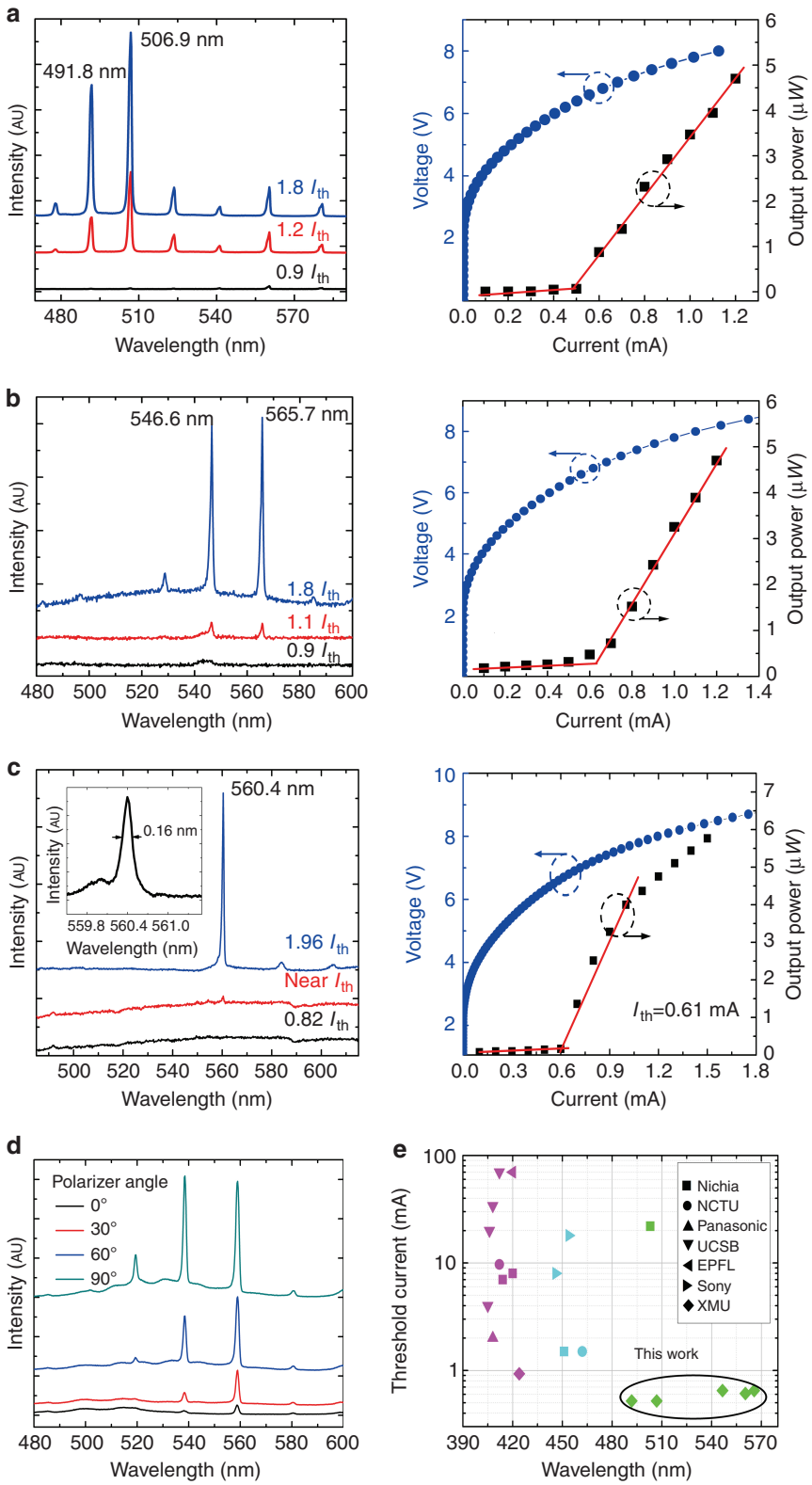

Figure 3 Room-temperature CW lasing characteristics. (**a**,**b**,**c**) are spectra at different current levels (left) and the corresponding voltage–current–light output characteristics (right) of three samples with different cavity lengths. (**d**) Polarization characteristics of the laser emission from another VCSEL at 1 mA. (**e**) Threshold current as a function of the wavelength for all electrically injected GaN-based VCSELs reported to date. Lasing spectra in **a**–**d** are offset along the *y* axis for clarity.

doi:10.1038/lsa.2016.199

The green VCSELs obtained in this study feature a low-threshold current density, low-thermal resistance and CW lasing. These properties are essential for practical applications. We mainly attribute the low-threshold current to the use of QDs as the active layer, in addition to the control of the optical loss in the cavity[43]. Low-dimensional nanoscale QDs are known to enhance the emission efficiency of the active layer due to the strong quantum confinement effect or carrier localization[29–31]. It has been reported that the strain effect is significantly reduced in InGaN QDs[28]. In our previous work, we reported a large localization energy of 105.9 meV and a high internal quantum efficiency of 41.1% for our InGaN QDs[44]. The strong carrier localization also suppresses nonradiative recombination by impeding carriers from being captured by defects outside the QD. Moreover, compared with GaAs, the advantage of using QD is more significant in GaN because the threshold current depends on the effective masses of the carriers. The transparency carrier density of a semiconductor material and the threshold carrier density of a semiconductor laser are, respectively, given by[45]

$$n_{tr} = 2\left(\frac{m_c^*}{m_0}\right)^{3/4}\left(\frac{m_v^*}{m_0}\right)^{3/4}\left(\frac{2\pi m_0 k_B T}{h^2}\right)^{3/2}$$

$$n_{th} = \left(\frac{\gamma_{th}}{a}\right) + n_{tr}$$

where m_c^* is the electron effective mass, m_v^* is the hole effective mass, m_0 is the free electron mass, k_B is Boltzmann's constant, h is Planck's constant and T is the temperature. γ_{th} and a are the threshold gain and differential gain, respectively. We can see that the effective masses of the carriers have a great effect on the value of n_{tr} and thereby n_{th}. For the well-studied semiconductor lasing material GaAs, n_{tr} is calculated to be $1.8\times10^{18}\,\mathrm{cm}^{-3}$ at 300 K ($m_c^* = 0.067\,m_0$, $m_v^* = 0.45\,m_0$). On the other hand, for GaN with larger effective masses ($m_c^* = 0.2\,m_0$, $m_v^* = 1.1\,m_0$), n_{tr} is $8\times10^{18}\,\mathrm{cm}^{-3}$, much higher than that of GaAs. This suggests a higher threshold carrier density for the GaN-based laser compared with the GaAs-based laser. However, when QDs are used as the active media of semiconductor lasers, where a δ-function-like density of states is expected, the lasing property is finally independent on the effective mass of the carriers[26]. Hence, the use of QDs is more effective in GaN-based lasers and definitely contributes to the low-threshold current observed here.

In addition, the use of a small-area bottom DBR, metal bonding and a copper plate is also expected to significantly improve the thermal dissipation of VCSELs. This has an important role in the realization of CW lasing at room temperature. The efficiency of the thermal dissipation has been shown to be important in the realization of current-injection GaN-based VCSELs[37,46]. To understand the thermal behavior inside the devices, we systematically investigated the thermal characteristics of VCSELs, both theoretically and experimentally. We first calculated the heat distribution of the QD VCSELs by a finite element method (FEM) using a steady-state three-dimensional heat dissipation model[47–49]. The heat dissipation model is given by[47,48]

$$-\nabla(k\nabla T) = Q$$

$$k\nabla T = h(T_{inf} - T) + \varepsilon\sigma(T^4{}_{surr} - T^4)$$

where Q, k, T, h, ε and σ are the heat source density, thermal conductivity, initial temperature, heat transfer coefficient, surface emissivity and Stefan–Boltzmann constant, respectively. T_{inf} and T_{surr} are the ambient temperature and the surrounding temperature, respectively. The heat source density Q can be obtained from the experimentally measured L–I–V data by $Q = \frac{U_{th}I_{th}}{V}$, where U_{th}, I_{th} and V are the threshold current, threshold voltage and volume of the active region, respectively. The heat distribution of the device is shown in Figure 4a, and the maximum increase in the temperature of the active region was 4 K at the threshold. The thermal resistance (R_{th}) was calculated to be 879 $\mathrm{K\,W^{-1}}$ by $R_{th} = \Delta T/V_{th}\,I_{th}$, where T,T_{th} and V_{th} are the temperature, threshold current and voltage at the threshold, respectively. Next, we experimentally measured the thermal resistance of the VCSELs. The thermal resistance of the VCSEL is given by $R_{th} = \Delta T/\Delta P = \Delta\lambda/\Delta P/\Delta\lambda/\Delta T$, where T, P and λ are the temperature, net consumed injection power and emission wavelength, respectively[47].

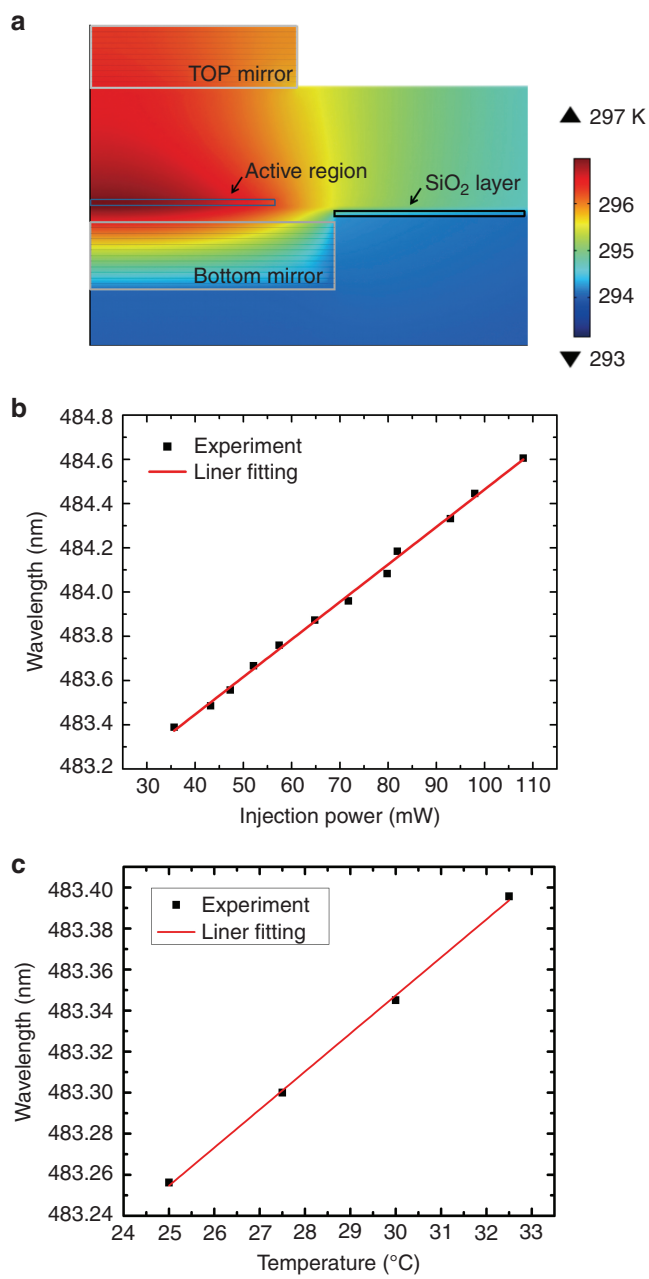

Figure 4 Thermal characteristics of the GaN-based VCSEL bonded on a copper plate. (**a**) Simulated temperature contours around the active region of the QD VCSEL at the threshold. The solid lines display the geometry of the different materials used in the simulation. (**b**) Lasing wavelength as a function of consumed injection power. (**c**) Wavelength versus temperature as measured with a thermoelectric cooler.

We first measured the movement of the lasing wavelength as a function of the substrate temperature. The injection current was set to 0.7 mA, slightly above the threshold, to avoid any current-heating effect, and the temperature of the substrate was controlled with a thermoelectric cooler. The measured dependence of the lasing wavelength on the temperature is shown in Figure 4b. On the other hand, the power-dependence of the lasing spectra for the same VCSEL was measured under different injection electric powers, as illustrated in Figure 4c. We can see clearly that the wavelength of the lasing peak moves linearly following both changes in the injection power and substrate temperature, with slopes of 0.169 Å mW^{-1} and 0.185 Å K^{-1}, respectively, which yields a thermal resistance of 915 K W^{-1}. This value is close to the calculated result and is much lower than the 2600 K W^{-1} reported for GaAs-based VCSELs with the same active region diameter[49]. A smaller thermal resistance indicates a higher ability of heat dissipation.

The lasing wavelength of 565.7 nm was the longest ever reported for GaN-based VCSELs. It is worth noting that this wavelength is near the edge of the PL emission band, where the gain should be not so high. The lasing is due to the strong coupling between electrons and photons, that is, the large overlap between the active region and the anti-nodes of the optical field of the standing-wave pattern in the cavity. A better overlap means a larger gain enhancement factor, which can effectively decrease the threshold gain of the VCSEL. The gain enhancement factor, defined as the optical density in the active layer normalized to that in the cavity, is given by[50]

$$\Gamma_r = \frac{L}{d_a}\frac{\int_{d_a}|E(z)|^2 dz}{\int_L |E(z)|^2 dz}$$

where L, d_a $E(z)$ are the cavity length, thickness of the active region and optical field standing-wave pattern, respectively. For VCSEL operation, the threshold gain is defined as[50]

$$G_{th} = \alpha_a + \frac{1}{\Gamma_r d_a}[\alpha_i(L_{eff} - d_a) + \ln\frac{1}{\sqrt{R_t R_b}}]$$

where α_a and α_i represent the loss coefficients of the active layer and the inner cavity excluding the active region, respectively, and L_{eff}, R_t and R_b are the effective cavity length and the reflectivity of the top and bottom mirrors, respectively. From the equation, we can see clearly that Γ_r has a remarkable influence on the threshold gain of VCSELs, especially when the thickness of the active region is small. The distribution of the optical field (squared electric field) of the 565.7-nm mode was calculated using the transfer matrix method and is shown in Figure 5a with the refractive index of the layers in the VCSEL. The accurate overlap between the active region and the antinode of the standing wave leads to a large gain enhancement, and Γ_r is estimated to be 1.982, which can explain the occurrence of the lasing action at the edge of the PL emission spectrum. For comparison, Γ_r is estimated to be 0.0235 when the active region is placed at the node of the standing wave.

Changing the cavity length shifts the optical field in the cavity and thereby modulates the coupling strength between the active layer and the optical fields of the different cavity modes. The enhancement factor and the lasing wavelength can be adjusted. The mode separations between the two adjacent cavity modes for the samples shown in Figure 3 are 15.1, 19.9, 24 and 20.41 nm, respectively, corresponding to cavity lengths of 3041, 2910, 2652 and 2807 nm, respectively. Adjusting the lasing wavelength by changing the cavity length is unique to VCSELs, as it is not possible for EELs. By using several VCSELs lasing at different wavelengths in the 'green gap' instead of the conventional RGB lasers, a larger gamut can be obtained for laser displays and projectors that can be extended to nearly 100% coverage of human vision. A CIE triangle of the HDTV gamut is given for comparison in Figure 5b. Thus, the laser lights from 490 nm (blue-green) to 560 nm (green-yellow) obtained in this study could be essential for the realization of wide-gamut compact displays and projectors.

We did not perform specialized testing on the device operation lifetime because the VCSEL was not separated and packaged. Nevertheless, the investigated devices seemed to be very stable in output performance during the measurements we carried out, which usually lasted several hours. In addition, after performing many measurements, the devices did not exhibit an observable performance deterioration; they broke down after many cycles of testing only after approximately half a year.

CONCLUSIONS

In conclusion, we have demonstrated room temperature, CW and low-threshold green lasing from InGaN QD-based VCSELs for the first time. The lasing wavelength extends from 491.8 nm (blue-green) to 565.7 nm (yellow-green), covering most of the 'green gap'. The thermal resistance of the VCSEL is as low as 915 K W^{-1}. For different VCSELs, the same QD active region was used with the wavelengths controlled by adjusting the cavity length. This is

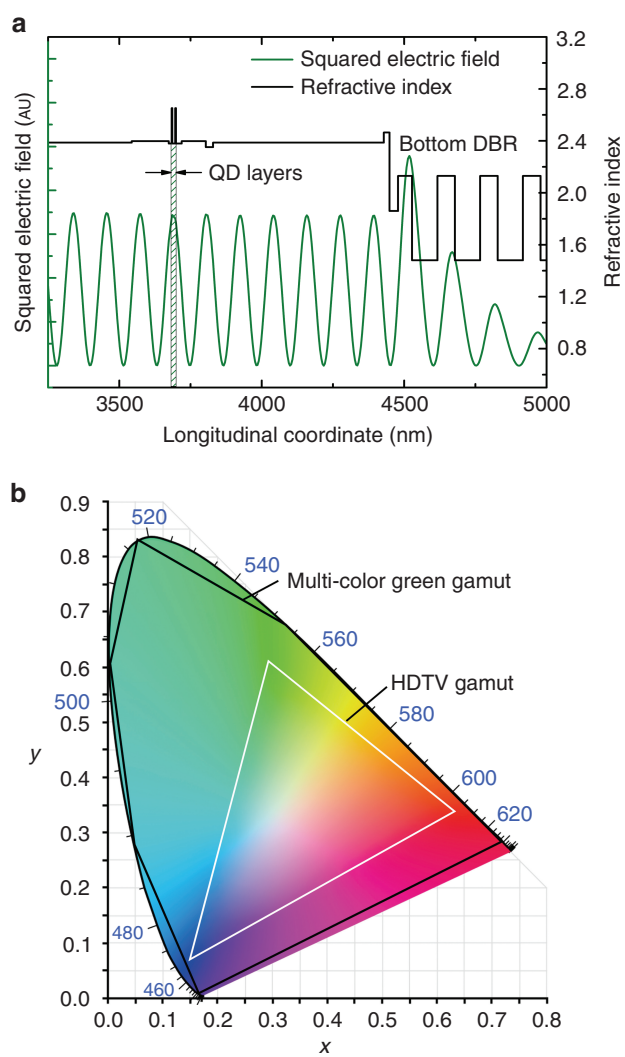

Figure 5 (**a**) Calculated electric field distribution for the 565.7 nm mode in the inner cavity of DM2. (**b**) Comparison of CIE HDTV (white triangle) and multi-color green (black polygon) color gamuts on a CIE 1931 *xy* chromaticity diagram.

doi:10.1038/lsa.2016.199

impossible in the case of EELs. Our results open up opportunities to design and fabricate semiconductor green lasers with excellent performance that may lead to wide-gamut compact displays and projectors. The VCSELs could also be bonded onto Si for integration with other optoelectronic devices/circuits.

CONFLICT OF INTEREST

The authors declare no conflict of interest.

AUTHOR CONTRIBUTIONS

The manuscript was written through the contributions of all the authors. All authors have given approval to the final version of the manuscript.

ACKNOWLEDGEMENTS

This work was supported by the National Natural Science Foundation of China (Grant Nos. 61274052, 11474235, U1505253), the Major Scientific and Technological Special Project of Guangdong Province (No. 2014B010119004) and the Science Challenge Project (No. JCKY2016212A503).

1 Hall RN, Fenner GE, Kingsley JD, Soltys TJ, Carlson RO. Coherent light emission from GaAs junctions. *Phys Rev Lett* 1962; **9**: 366–368.
2 Nathan MI, Dumke WP, Burns G, Dill FH, Lasher G. Stimulated emission of radiation from GaAs *p-n* junctions. *Appl Phys Lett* 1962; **1**: 62–64.
3 Mokkapati S, Jagadish C. III-V compound SC for optoelectronic devices. *Materials Today* 2009; **12**: 22–32.
4 Yin ZY, Tang XH. A review of energy bandgap engineering in III-V semiconductor alloys for mid-infrared laser applications. *Solid-State Electron* 2007; **51**: 6–15.
5 Lee TP. Recent advances in long-wavelength semiconductor lasers for optical fiber communication. *Proc IEEE* 1991; **79**: 253–276.
6 Tilma BW, Mangold M, Zaugg CA, Link SM, Waldburger D *et al.* Recent advances in ultrafast semiconductor disk lasers. *Light: Sci Appl* 2015; **4**: e310, doi:10.1038/lsa.2015.83.
7 Keller U. Recent developments in compact ultrafast lasers. *Nature* 2003; **424**: 831–838.
8 Moser P, Lott JA, Larisch G, Bimberg D. Impact of the oxide-aperture diameter on the energy efficiency, bandwidth, and temperature stability of 980-nm VCSELs. *J Lightwave Technol* 2015; **33**: 825–831.
9 Kryuchyn AA, Petrov VV, Kostyukevych SO. High density optical recording in thin chalcogenide films. *J Optoelectr Adv Mater* 2011; **13**: 1487–1492.
10 Rothenbach CA, Gupta MC. High resolution, low cost laser lithography using a Blu-ray optical head assembly. *Optics Lasers Eng* 2012; **50**: 900–904.
11 Wierer Jr JJ, Tsao JY, Sizov DS. Comparison between blue lasers and light-emitting diodes for future solid-state lighting. *Laser Photonics Rev* 2013; **7**: 963–993.
12 Zhang YF, Dong H, Wang R, Duan JY, Shi AC *et al.* Demonstration of a home projector based on RGB semiconductor lasers. *Appl Opt* 2012; **51**: 3584–3589.
13 Fujita S. Wide-bandgap semiconductor materials: for their full bloom. *Jpn J Appl Phys* 2015; **54**: 030101.
14 Haase MA, Qiu J, DePuydt JM, Cheng H. Blue-green laser diodes. *Appl Phys Lett* 1991; **59**: 1272–1274.
15 Kasai J, Akimoto R, Hasama T, Ishikawa H, Fujisaki S *et al.* Green-to-yellow continuous-wave operation of BeZnCdSe quantum-well laser diodes at room temperature. *Appl Phys Express* 2011; **4**: 082102.
16 Akasaki I. Fascinating journeys into blue light (Nobel Lecture). *Ann Phys* 2015; **527**: 311–326.
17 Nakamura S. Background story of the invention of efficient blue InGaN light emitting diodes (Nobel Lecture). *Ann Phys* 2015; **527**: 335–349.
18 Miyoshi T, Masui S, Okada T, Yanamoto T, Kozaki T *et al.* 510–515 nm InGaN-based green laser diodes on *c*-plane GaN substrate. *Appl Phys Express* 2009; **2**: 062201.
19 Lutgen S, Avramescu A, Lermer T, Queren D, Müller J *et al.* True green InGaN laser diodes. *Phys Status Solidi A* 2010; **207**: 1318–1322.
20 Enya Y, Yoshizumi Y, Kyono T, Akita K, Ueno M *et al.* 531nm green lasing of InGaN based laser diodes on semi-polar {20-21} free-standing GaN substrates. *Appl Phys Express* 2009; **2**: 082101.
21 Sizov DS, Bhat R, Zakharian A, Napierala J, Song KC *et al.* Impact of carrier transport on aquamarine-green laser performance. *Appl Phys Express* 2010; **3**: 122101.
22 Lin YD, Yamamoto S, Huang CY, Hsiung CL, Wu F *et al.* High quality InGaN/AlGaN multiple quantum wells for semipolar InGaN green laser diodes. *Appl Phys Express* 2010; **3**: 082001.
23 Wu XH, Fini P, Tarsa EJ, Heying B *et al.* Dislocation generation in GaN heteroepitaxy. *J Cryst Growth* 1998; **189-190**: 231–243.
24 Takeuchi T, Sota S, Katsuragawa M, Komori M, Takeuchi H *et al.* Quantum-confined stark effect due to piezoelectric fields in GaInN strained quantum wells. *Jpn J Appl Phys* 1997; **36**: L382–L385.
25 Funato M, Kim YS, Ochi Y, Kaneta A, Kawakami Y *et al.* Optical gain spectra of a (0001) InGaN green laser diode. *Appl Phys Express* 2013; **6**: 122704.
26 Sizov D, Bhat R, Wang J, Zah CE. Reliability and degradation of InAlGaN semipolar (20-21) plane green lasers with relaxed InGaN waveguide core. *Appl Phys Express* 2014; **7**: 112701.
27 Lin YD, Hardy MMT, Hsu PS, Kelchner KM, Huang CY *et al.* Blue-green InGaN/GaN laser diodes on miscut *m*-plane GaN substrate. *Appl Phys Express* 2009; **2**: 082102.
28 Schulz S, O'Reilly EP. Theory of reduced built-in polarization field in nitride-based quantum dots. *Phys Rev B* 2010; **82**: 033411.
29 Arakawa Y. Progress in GaN-based quantum dots for optoelectronics applications. *IEEE J Sel Topics Quantum Electron* 2002; **8**: 823–832.
30 Ledentsov NN, Bimberg D, Alferov ZI. Progress in epitaxial growth and performance of quantum dot and quantum wire lasers. *J Lightwave Technol* 2008; **26**: 1540–1555.
31 Wu J, Chen SM, Seeds A, Liu HY. Quantum dot optoelectronic devices: lasers, photodetectors and solar cells. *J Phys D: Appl Phys* 2015; **48**: 363001.
32 Zhang M, Banerjee A, Lee CS, Hinckley JM, Bhattacharya P. A InGaN/GaN quantum dot green (lambda = 524 nm) laser. *Appl Phys Lett* 2011; **98**: 221104.
33 Chang-Hasnain CJ. VCSELs advances and future prospects. *Opt Photon News* 1998; **9**: 34–39.
34 Bhattacharya P, Banerjee A, Frost T. InGaN/GaN quantum dot blue and green lasers. *Proc of SPIE* 2013; **8640**: 86400J.
35 Lu TC, Chen SW, Wu TT, Tu PM, Chen CK *et al.* Continuous wave operation of current injected GaN vertical cavity surface emitting lasers at room temperature. *Appl Phys Lett* 2010; **97**: 071114.
36 Kasahara D, Morita D, Kosugi T, Nakagawa K, Kawamata J *et al.* Demonstration of blue and green GaN-based vertical-cavity surface-emitting lasers by current injection at room temperature. *Appl Phys Express* 2011; **4**: 072103.
37 Liu WJ, Hu XL, Ying LY, Zhang JY, Zhang BP. Room temperature continuous wave lasing of electrically injected GaN-based vertical cavity surface emitting lasers. *Appl Phys Lett* 2014; **104**: 251116.
38 Holder C, Speck JS, DenBaars SP, Nakamura S, Feezell D. Demonstration of nonpolar GaN-based vertical-cavity surface-emitting lasers. *Appl Phys Express* 2012; **5**: 092104.
39 Onishi T, Imafuji O, Nagamatsu K, Kawaguchi M, Yamanaka K *et al.* Continuous wave operation of GaN vertical cavity surface emitting lasers at room temperature. *IEEE J Quantum Electron* 2012; **48**: 1107–1112.
40 Izumi S, Fuutagawa N, Hamaguchi T, Murayama M, Kuramoto M *et al.* Room-temperature continuous-wave operation of GaN-based vertical-cavity surface-emitting lasers fabricated using epitaxial lateral overgrowth. *Appl Phys Express* 2015; **8**: 062702.
41 Li ZC, Liu JP, Feng MX, Zhou K, Zhang SM *et al.* Effects of matrix layer composition on the structural and optical properties of self-organized InGaN quantum dots. *J Appl Phys* 2013; **114**: 093105.
42 Moriwaki O, Someya T, Tachibana K, Ishida S, Arakawa Y. Narrow photoluminescence peaks from localized states in InGaN quantum dot structures. *Appl Phys Lett* 2000; **76**: 2361–2363.
43 Ying LY, Hu XL, Liu WJ, Zhang JY, Zhang BP *et al.* Control of optical loss in GaN-based planar cavities. *Superlattice Microst* 2015; **88**: 561–566.
44 Weng GE, Zhao WR, Chen SQ, Akiyama H, Li ZC *et al.* Strong localization effect and carrier relaxation dynamics in self-assembled InGaN quantum dots emitting in the green. *Nanoscale Res Lett* 2015; **10**: 31.
45 Lu TC, Wang SC (in Chinese). Introduction to semiconductor Lasers. In: *Optical Gain and Amplifier*. Wu-Nan Book Inc; 2008. pp 264–266.
46 Liu WJ, Hu XL, Ying LY, Chen SQ, Zhang JY *et al.* On the importance of cavity-length and heat dissipation in GaN-based vertical-cavity surface-emitting lasers. *Sci Rep* 2015; **5**: 9600.
47 Wang JH, Savidis I, Friedman EG. Thermal analysis of oxide-confined VCSEL arrays. *Microelectron J* 2011; **42**: 820–825.
48 Lee HK, Song YM, Lee YT, Yu JS. Thermal analysis of asymmetric intracavity-contacted oxide-aperture VCSELs for efficient heat dissipation. *Solid-State Electron* 2009; **53**: 1086–1091.
49 MacDougal MH, Geske J, Lin CK, Bond AE, Dapkus PD. Thermal Impedance of VCSEL's with AlO-GaAs DBR's. *IEEE Photon Technol Lett* 1998; **10**: 15–17.
50 Michalzik R. *Fundamentals, Technology and Applications of Vertical-Cavity Surface-Emitting Lasers*. Berlin: Springer; 2013. pp 27–30.

This work is licensed under a Creative Commons Attribution-NonCommercial-ShareAlike 4.0 International License. The images or other third party material in this article are included in the article's Creative Commons license, unless indicated otherwise in the credit line; if the material is not included under the Creative Commons license, users will need to obtain permission from the license holder to reproduce the material. To view a copy of this license, visit http://creativecommons.org/licenses/by-nc-sa/4.0/

© The Author(s) 2017